

Unreliability of two-band model analysis of magnetoresistivities in unveiling temperature-driven Lifshitz transition

Jing Xu,^{1,2} Yu Wang,³ Samuel E. Pate,^{1,4} Yanglin Zhu ,³ Zhiqiang Mao,³ Xufeng Zhang,² Xiuquan Zhou,¹ Ulrich Welp,¹ Wai-Kwong Kwok,¹ Duck Young Chung,¹ Mercouri G. Kanatzidis,^{1,5} and Zhi-Li Xiao ^{1,4,*}

¹Materials Science Division, Argonne National Laboratory, Argonne, Illinois 60439, USA

²Center for Nanoscale Materials, Argonne National Laboratory, Argonne, Illinois 60439, USA

³Department of Physics, Pennsylvania State University, University Park, Pennsylvania 16802, USA

⁴Department of Physics, Northern Illinois University, DeKalb, Illinois 60115, USA

⁵Department of Chemistry, Northwestern University, Evanston, Illinois 60208, USA



(Received 20 September 2022; accepted 23 December 2022; published 4 January 2023)

Recently, anomalies in the temperature dependences of the carrier density and/or mobility derived from analysis of the magnetoresistivities using the conventional two-band model have been used to unveil intriguing temperature-induced Lifshitz transitions in various materials. For instance, two temperature-driven Lifshitz transitions were inferred to exist in the Dirac nodal-line semimetal ZrSiSe, based on two-band model analysis of the Hall magnetoconductivities where the second band exhibits a change in the carrier type from holes to electrons when the temperature decreases below $T = 106$ K and a dip is observed in the mobility vs temperature curve at $T = 80$ K. Here, we revisit the experiments and two-band model analysis on ZrSiSe. We show that the anomalies in the second band may be spurious because the first band dominates the Hall magnetoconductivities at $T > 80$ K, making the carrier type and mobility obtained for the second band from the two-band model analysis unreliable. That is, care must be taken in interpreting these anomalies as evidence for temperature-driven Lifshitz transitions. Our skepticism on the existence of such phase transitions in ZrSiSe is further supported by the validation of Kohler's rule for magnetoresistances for $T \leq 180$ K. In this paper, we showcase potential issues in interpreting anomalies in the temperature dependence of the carrier density and mobility derived from the analysis of magnetoconductivities or magnetoresistivities using the conventional two-band model.

DOI: [10.1103/PhysRevB.107.035104](https://doi.org/10.1103/PhysRevB.107.035104)

I. INTRODUCTION

As an electronic topological transition without lattice symmetry breaking, the Lifshitz transition, at which the Fermi surface (FS) topology changes due to the variation of the Fermi energy and the band structure [1,2], has attracted extensive attention recently [2–24]. It can be induced by various parameters such as pressure and magnetic field in a variety of materials including superconductors as well as topological materials [2–17]. For example, magnetic field-induced Lifshitz transitions were observed in UCoGe [2] and CeIrIn₅ [5]. Black phosphorus [3] and ZrSiTe [4] exhibit Lifshitz transitions under pressures. Ba(Fe_{1-x}Co_x)₂As₂ [6] and V_{1-x}Ti_xAl₃ [7] were found to undergo Lifshitz transitions at the doping levels of $x = 0.038$ and 0.35 , respectively. Temperature-induced Lifshitz transitions were reported in WTe₂ [8], ZrTe₅ [9], ZrSiSe [10], InTe_{1- δ} [11], Ag₂Se [12], Nb₂Se₃ [13], and ZrSiTe [14]. Surface charge doping can also induce a Lifshitz transition in NbAs [15]. Ultrafast dynamical Lifshitz transitions can even be induced by photons in MoTe₂ [16] and ZrSiTe [17].

Angle-resolved photoemission spectroscopy, which can probe direct information on the FS and electronic struc-

ture of materials, has been the most common experimental technique in revealing Lifshitz transitions [6,8,9,15–18]. de Haas–van Alphen [2] and Shubnikov–de Haas [3,5] quantum oscillations also have been used to investigate Lifshitz transitions by probing the change in the FS topology. Methods such as Raman spectroscopy [4] and nuclear magnetic resonance spectroscopy [14] also have been used, though they can only detect Lifshitz transition-induced anomalies in other properties rather than the changes in the FS and the band structure. Recently, conventional transport measurements on the longitudinal resistivity ρ_{xx} and/or the Hall resistivity ρ_{xy} [7,10–13,19–24] have been increasingly utilized to uncover Lifshitz transitions since the change in FS topology can result in anomalies in the evolution of the carrier density n and/or mobility μ , for example, with doping [7,19] or temperature [10–13,20–24].

In this paper, we intend to show that, whereas a Lifshitz transition can induce anomalies in n and μ , the converse may not necessarily be correct. For example, such anomalies could also arise from the change in the shape and size of the FS in the absence of a Lifshitz transition. Below, we reveal that artificial anomalies may also occur in multiband materials due to the lack of a reliable determination of the density and mobility values obtained from transport measurements. Currently, n and μ are obtained from (i) the Hall resistivity ρ_{xy} using the single-band picture [11,12] and (ii) the two-band model

*xiao@anl.gov

fits on the Hall magnetoconductivity σ_{xy} [10,19–21,24], Hall magnetoresistivity ρ_{xy} [22,23], or simultaneously on both the Hall and longitudinal magnetoconductivities σ_{xx} and σ_{xy} converted from the measured magnetoresistivities ρ_{xx} and ρ_{xy} [13].

In the first method, for a single-band (or one dominant band) system, the Hall resistivity ρ_{xy} is proportional to the magnetic field H , i.e., $\rho_{xy} = R_H H$, where R_H is the Hall coefficient. The carrier density can be calculated using $n_H = 1/(eR_H)$, and the mobility μ can be derived using $\mu = R_H/\rho_{xx}(0)$, with $\rho_{xx}(0)$ being the longitudinal resistivity at zero field [11]. As discussed in Ref. [25], however, a linear relationship between ρ_{xy} and H can also exist in a two-band or multiband material with varying mobilities among different bands if $\mu_i H \ll 1$, where μ_i is the carrier mobility of the i th band. Furthermore, a compensated two-band system can always have a linear dependence of ρ_{xy} on H , regardless of the values of the carrier mobilities and the magnetic field. In this case, the value of n/n_H depends on the ratio of the mobilities in the two bands. That is, the values estimated using the single-band picture can differ from the carrier density and mobility in the material. Thus, their anomalies such as peaks/discontinuity in the temperature dependence of n and μ may not reflect Lifshitz transitions.

Here, we tackle the suitability of the second method, i.e., using the anomalies in the evolution of the carrier densities and mobilities derived from two-band model fittings of the experimental magnetoresistivities/magnetoconductivities as evidence for a Lifshitz transition. We revisit the temperature-driven Lifshitz transition recently reported by Chen *et al.* [10] in ZrSiSe, using deduction from anomalies in the temperature dependence of the carrier density and mobility derived by analyzing the Hall magnetoconductivity σ_{xy} using the two-band model. We conduct the same measurements and data analysis on ZrSiSe and show that the observed anomalies may not represent evidence for a temperature-driven Lifshitz transition. We also find that the magnetoresistivities ρ_{xx} obey Kohler's rule that is valid only when the carrier density is temperature insensitive [25], casting further doubts on the existence of a temperature-induced Lifshitz transition in ZrSiSe.

II. MATERIALS AND METHODS

We conducted resistance measurements on two plate-like ZrSiSe crystals grown using a chemical vapor transport method [26]. Electrical leads were gold wires glued to the crystal using silver epoxy H20E. The magnetic field is applied along the c axis of the crystal, while the current flows in the ab plane, i.e., the magnetic field is always perpendicular to the current. We measured both longitudinal and Hall resistance $R_{xx}(H)$ and $R_{xy}(H)$ curves at various fixed temperatures, enabling the calculation of the magnetoresistivities $\rho_{xx}(H) = R_{xx} w d / l$ and $\rho_{xy}(H) = R_{xy} d$, where w , d , and l are the width, thickness of the sample, and the separation between the voltage contacts, respectively. They were converted into magnetoconductivities using equations $\sigma_{xy} = \rho_{xy}/(\rho_{xx}^2 + \rho_{xy}^2)$ and $\sigma_{xx} = \rho_{xx}/(\rho_{xx}^2 + \rho_{xy}^2)$ [10]. The magnetoresistance is defined as $MR = [\rho_{xx}(H) - \rho_0]/\rho_0$, where ρ_{xx} and ρ_0 are the resistivities at a fixed temperature with and without the presence of a magnetic field, respectively. We used Origin 2021b

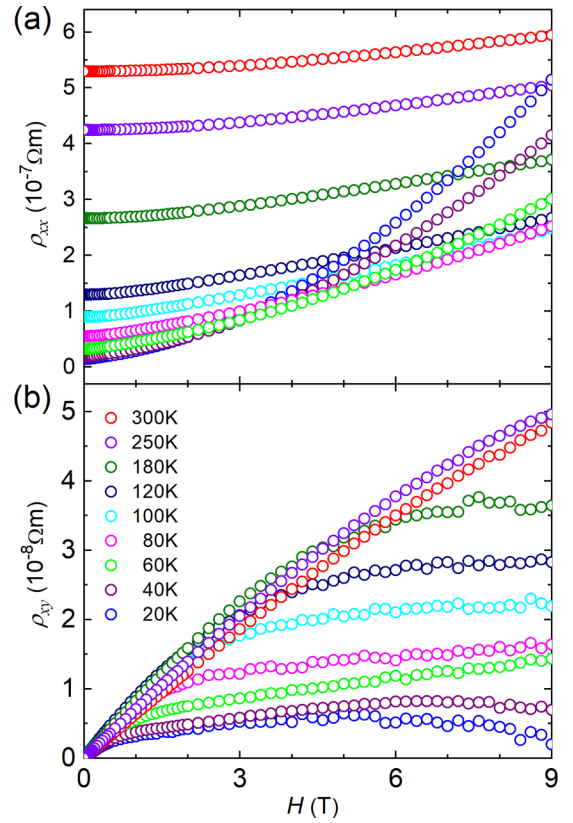


FIG. 1. Magnetic field dependence of (a) the longitudinal magnetoresistivity $\rho_{xx}(H)$ and (b) the Hall magnetoresistivity $\rho_{xy}(H)$ obtained at various temperatures (for clarity, curves for $T < 20$ K are omitted since they are nearly indistinguishable to that for $T = 20$ K). The data were taken at $H \parallel c$ and the current flows in the ab plane. The residual resistivity ratio of the sample, $RRR = \rho_0(300\text{K})/\rho_0(3\text{K})$, is 39. Symbols for data taken at various temperatures are the same in both (a) and (b).

from OriginLab Corporation [27] in data plotting and analysis including the fittings presented below.

III. RESULTS AND DISCUSSION

We measured two samples which exhibit similar behavior, with data from one of them presented here. Figures 1(a) and 1(b) show the magnetic field dependences of the longitudinal resistivity $\rho_{xx}(H)$ and Hall resistivity $\rho_{xy}(H)$ at various temperatures, which resemble those reported in Ref. [10]. For example, the $\rho_{xy}(H)$ curves exhibit the reported three characteristic features, including the increased nonlinearity as the temperature is lowered, positive slope for $T > 40$ K, and a slope change in the curves for $T \leq 40$ K. The measured $\rho_{xx}(H)$ and $\rho_{xy}(H)$ enable the calculation of the magnetoconductivities, as presented in Figs. 2(a) and 2(c) for σ_{xy} and Figs. 2(b) and 2(d) for σ_{xx} for $T = 20$ and 300 K, respectively (see Fig. S1 in the Supplemental Material [28] for all σ_{xy} curves calculated from data in Fig. 1, which show a similar trend with temperature as those in Fig. 2(c) of Ref. [10]).

As discussed by Chen *et al.* [10], the slope of the $\rho_{xy}(H)$ curve may provide qualitative information on the relative contributions of the two carrier types. For example, a

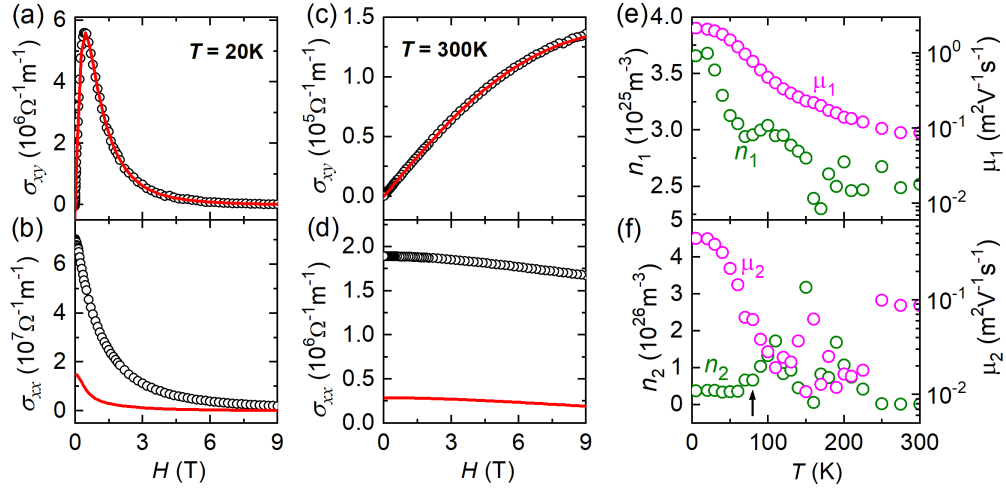


FIG. 2. Two-band model analysis of Hall magnetoconductivities $\sigma_{xy}(H)$. (a) and (c) show examples of fits (red lines) of Eq. (1) to experimental results (black circles) at $T = 20$ and 300 K, respectively. (b) and (d) compare the calculated longitudinal magnetoconductivities $\sigma_{xx}(H)$ (red lines) using the fitting parameters obtained in (a) and (c) with the experimental data (black circles). The large separation between the red lines and the black circles in (b) and (d) indicates that the parameters obtained in fitting $\sigma_{xy}(H)$ do not describe the $\sigma_{xx}(H)$ properly (see more discussions in the text). (e) and (f) show the temperature dependence of the derived fitting parameters for the first (n_1 , μ_1) and the second (n_2 , μ_2) bands, respectively. The fluctuation of the fitting parameters, particularly n_2 and μ_2 in (f) at $T > 80$ K, is due to the negligible contribution $\sigma_{xy,2}$ of the second band in Eq. (1) to the total magnetoconductivity $\sigma_{xy}(H)$. The arrow in (f) marks the temperature of $T = 80$ K.

positive slope may indicate the dominance of the holes in the electronic transport. Quantitatively, they obtained the carrier density and mobility by applying the conventional two-band model on the Hall magnetoconductivity, which can be expressed as

$$\sigma_{xy}(H) = e \left(\frac{n_1 \mu_1^2}{1 + \mu_1^2 H^2} - \frac{n_2 \mu_2^2}{1 + \mu_2^2 H^2} \right) H, \quad (1)$$

where e is the charge of the electron, and n_1 and n_2 are the densities and μ_1 and μ_2 are mobilities of the carriers in the first and second bands, respectively. Note that we apply a minus sign to the second term in Eq. (1) so that the derived n_2 for the electron band will be positive rather than negative in Ref. [10], as required in the calculation of $\sigma_{xx}(H)$ presented below.

By fitting the experimental $\sigma_{xy}(H)$ curves obtained at various temperatures using Eq. (1), Chen *et al.* [10] found that the second band exhibits a change in the carrier type from holes at $T > 106$ K to electrons at $T < 106$ K and a dip in the mobility vs temperature curve at $T = 80$ K. Along with other characterizations, they concluded that the temperature induces two Lifshitz transitions, at $T = 80$ and 106 K, respectively.

Here, we do not aim to prove that Lifshitz transitions do not exist in ZrSiSe. We are also not against using the two-band model fitting to estimate the carrier density and mobility in two-band [29] and multiband materials [10,13,19–24]. Instead, we focus on demonstrating that the two-band model fitting, though it limits the free parameters to four, can result in uncertain outcomes for ZrSiSe. We urge caution to be taken when drawing conclusions on a multiband system from the carrier density and mobility derived from the two-band model, such as claiming Lifshitz transitions based on anomalies in their temperature dependence.

We followed the same analysis procedure, i.e., using Eq. (1) to fit the $\sigma_{xy}(H)$ curves for various temperatures to obtain the carrier density and mobility. As presented in Figs. 2(a) and 2(c) for $T = 20$ and 300 K as examples, Eq. (1) can indeed describe the experimental data very well. The derived carrier densities and mobilities at various temperatures for the first and second bands are presented in Figs. 2(e) and 2(f), respectively. While both the values and the temperature dependence of the carrier density and mobility for the first band are consistent with those reported in Ref. [10], anomalies indeed occur at $T \sim 80$ K in the temperature dependence of the carrier density and mobility of the second band: at $T \leq 80$ K, n_2 and μ_2 smoothly decrease with increasing temperature, and their values are comparable with those (n_1 and μ_1) of the first band. On the other hand, the values of both n_2 and μ_2 for $T > 80$ K seem to be random, with n_2 being 1 order of magnitude larger than those of n_1 . The randomness of the n_2 and μ_2 values indicates that four free parameters in Eq. (1) are too many for the fittings since the fits did not converge, indicating the existence of mutual dependency between parameters [27]. In fact, the values of μ_2 are orders of magnitude smaller than those of μ_1 , resulting in the value ($\sigma_{xy,2}$) of the second term being much smaller than that ($\sigma_{xy,1}$) of the first term in Eq. (1). This can be seen clearly in Fig. 3, showing that the ratio of $\sigma_{xy,2}/\sigma_{xy,1}$ depends on both the temperature and magnetic field. At low temperatures, the second term $\sigma_{xy,2}$ contributes significantly to the total value, though it never overwhelms the first term. At high temperatures, the contribution of the second term is negligible, e.g., $< 4\%$ of that of the first term for $T \geq 180$ K. That is, n_2 and μ_2 can be any values if $\sigma_{xy,2}$ is negligible. This implies that Hall magnetoconductivities $\sigma_{xy}(H)$ at high temperatures can be described with only the first term, i.e., reducing the two-band model to a one-band model. In Fig. 4(b), we present one-band fittings of the $\sigma_{xy}(H)$ curves for various temperatures, showing good overlaps and

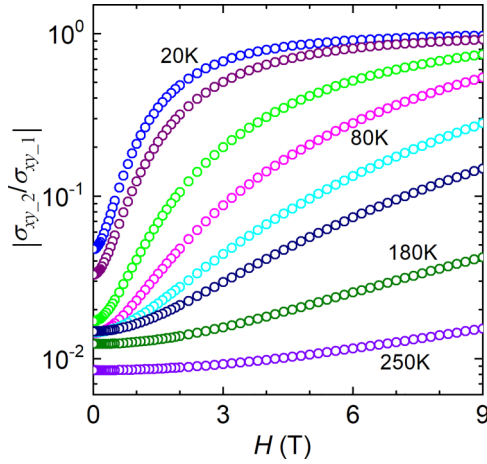


FIG. 3. Magnetic field dependence of the ratio of the magnetoconductivity $\sigma_{xy,2}$ of the second band to that ($\sigma_{xy,1}$) of the first band in the two-band model analysis Eq. (1), where $\sigma_{xy,i} = en_i\mu_i^2H/[1 + (\mu_iH)^2]$ with $i = 1$ and 2. The symbols are the same as those in Fig. 1.

significant disparities between the fitting curves and experimental data obtained at high ($T = 250$ and 100 K) and low ($T = 80$ and 20 K) temperatures, respectively. To better reveal the temperature effects on the fitting, we present in Fig. 4(a)

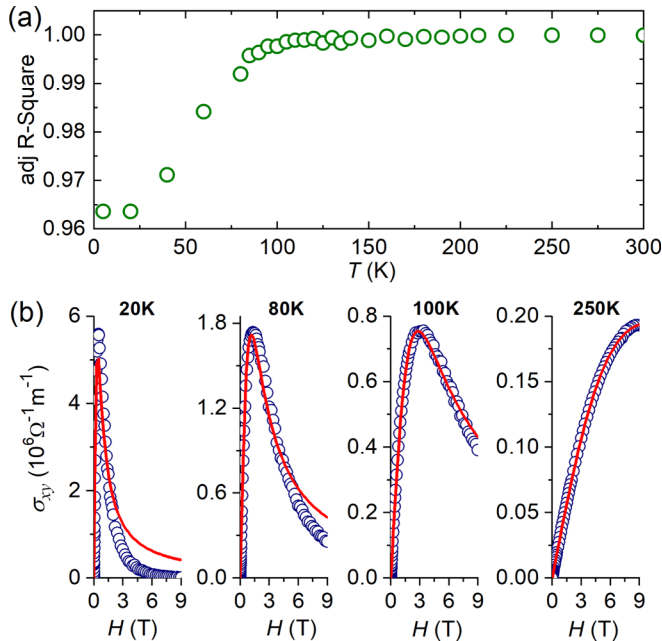


FIG. 4. (a) Temperature dependence of the Adj. R-square obtained in one-band fittings of the experimental σ_{xy} , i.e., by setting n_2 and μ_2 in Eq. (1) to be 0. Here, Adj. R-square is a modified version of R-square that is also known as the coefficient of determination (COD). It is a statistical measure to qualify the linear regression and is always < 1 . The larger the Adj. R-square, the better the fit. When the Adj. R-square approaches 1, the fitted line explains all the variability of the response data around its mean [30]. (b) Examples showing the quality of the one-band fittings at various temperatures. The blue circles represent experimental σ_{xy} , while red lines are the fits.

the temperature dependence of the Adj. R-square, which is a modified version of R-square and is used to quantify how well a model fits the data [30]. A value of less than but closer to 1 corresponds to a better fit. It indicates that at $T > 80$ K, the one-band model can describe the experimental $\sigma_{xy}(H)$ data very well, while the disparity becomes more pronounced with decreasing temperature for $T \leq 80$ K. This reaffirms that the anomalies (randomness in n_2 and μ_2) at $T > 80$ K are caused by too many free parameters in Eq. (1) in fitting the experimental data.

We note that the derived n_2 and μ_2 in Ref. [10] do not exhibit the randomness of those presented in Fig. 2(f), though in both cases, the anomalies concurrently occur at $T \approx 80$ K, and the values $\sigma_{xy,2}$ of the second term in Ref. [10] are also negligible for $T > 100$ K (because $n_2 \ll n_1$). It may be caused by the programs used for the fittings or the ways of parameter initialization, i.e., choosing the initial parameters to start the fittings. In any case, the outcomes of a fitting to only $\sigma_{xy}(H)$ with four free parameters need to be scrutinized. For this purpose, we present in Figs. 2(b) and 2(d) comparisons of the experimental $\sigma_{xx}(H)$ for $T = 20$ and 300 K with those calculated using the two-band model:

$$\sigma_{xx}(H) = e \left(\frac{n_1\mu_1}{1 + \mu_1^2 H^2} + \frac{n_2\mu_2}{1 + \mu_2^2 H^2} \right), \quad (2)$$

and the values of n_1 , μ_1 , n_2 , and μ_2 obtained in the $\sigma_{xy}(H)$ fittings in Figs. 2(a) and 2(c). The pronounced disparities clearly show potential issues related to obtaining the carrier density and mobility using a two-band model to fit only the $\sigma_{xy}(H)$ curves. This can be further illustrated by simultaneously fitting both $\sigma_{xx}(H)$ and $\sigma_{xy}(H)$ using Eqs. (1) and (2) of the two-band model, as presented in Fig. S2 in the Supplemental Material [28]. While the fits for $T = 300$ K are reasonably good, the fits for $T = 20$ K show significant disparity, as shown in Figs. S2(a) and S2(b) in the Supplemental Material [28]. The derived carrier densities and mobilities presented in Figs. S2(c) and S2(d) in the Supplemental Material [28] show different behavior from those in Figs. 2(e) and 2(f). This shows that a Lifshitz transition could occur at a different temperature if it were inferred from an anomaly in the temperature dependence of the carrier density. Thus, anomalies in the temperature dependence of the carrier density and mobility obtained through two-band model analysis of the magneto-transport data do not necessarily denote Lifshitz transitions.

Since ZrSiSe has three bands [26,31], we also analyzed the experimental data using a three-band model. Obviously, this approach cannot apply to only $\sigma_{xy}(H)$ since the two-band model fittings can already be overparameterized, as discussed above. Even when we fitted the $\sigma_{xy}(H)$ and $\sigma_{xx}(H)$ curves simultaneously by adding an electron band to Eqs. (1) and (2), the derived densities (n_1 , n_2 , and n_3) and mobilities (μ_1 , μ_2 , and μ_3) still depend on parameter initialization. On the other hand, if a hole band is added by using $\sigma_{xy}(H) = e \left(\frac{n_1\mu_1^2}{1 + \mu_1^2 H^2} - \frac{n_2\mu_2^2}{1 + \mu_2^2 H^2} + \frac{n_3\mu_3^2}{1 + \mu_3^2 H^2} \right) H$ and $\sigma_{xx}(H) = \sum_i \frac{en_i\mu_i}{1 + \mu_i^2 H^2}$, with $i = 1, 2$, and 3, the fits can produce repeatable values of the densities and mobilities. However, the disparities between the fit and the experimental curves can become even larger for $\sigma_{xy}(H)$, while those for $\sigma_{xx}(H)$ are indeed decreased, as shown in Fig. S4 in the Supplemental Material [28]. That said,

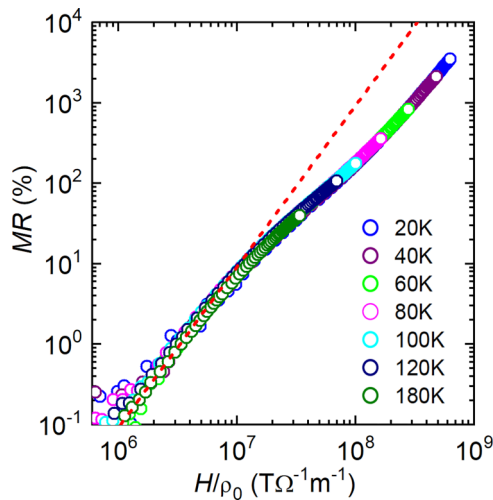


FIG. 5. Kohler's rule plots of longitudinal magnetoresistivity $\rho_{xx}(H)$ curves in Fig. 1, implying the absence of a temperature-driven Lifshitz transition at $T = 80\text{--}180$ K. The symbols are the same as those in Fig. 1. For clarity, only data up to $T = 180$ K are presented. Kohler's rule plots of all data from Fig. 1 and discussions on thermal-induced change in the carrier density are presented in the Supplemental Material [28]. The red dotted line represents $MR \sim (H/\rho_0)^2$.

fittings of the magnetoconductivity data, as demonstrated in both the two- and three-band model analyses, are not reliable methods to quantitatively determine the carrier density and mobility in a multiband semimetal. In other words, anomalies in the temperature dependence of the derived carrier density and mobility may not be associated with Lifshitz transitions.

To further demonstrate that the carrier density and mobility in ZrSiSe may have no anomalies in their temperature dependence, we conducted Kohler's rule analysis on the experimental data. As shown in Fig. 5, the MRs for $T \leq 180$ K obey Kohler's rule very well, consistent with that reported in Ref. [32]. The $MR \sim H/\rho_0$ relationship shows a similar behavior observed in other multiband semimetals [25,33], i.e., following a power law of $MR \sim (H/\rho_0)^\alpha$, with $\alpha = 2$ at low magnetic fields and deviating from it at higher field values. Since Kohler's rule is valid for systems with temperature-insensitive carrier densities [25], the scaling behavior in Fig. 5 suggests the absence of anomalies in the temperature dependence of the carrier density at $T \leq 180$ K. We note that the curve for $T = 180$ K shifts slightly to the right of that for $T = 120$ K. Such a deviation from Kohler's rule is caused by the small increase of the carrier density due to thermal activation, which becomes more pronounced at higher temperatures, as manifested by the curves for $T = 250$ and

300 K in Fig. S4(a) in the Supplemental Material [28]. It can be accounted for by a change in the thermal factor n_T in the extended Kohler's rule $MR \sim H/(n_T \rho_0)$ [25], as shown in Fig. S4(b) in the Supplemental Material [28], where values $n_T = 1.03, 1.11,$ and 1.18 are derived for $T = 180, 250,$ and 300 K, respectively, by assuming $n_T = 1$ for $T = 120$ K (and below).

IV. CONCLUSIONS

In summary, we have shown that anomalies in the temperature dependence of the carrier density and/or mobility derived from the analysis of magnetoconductivity using the conventional two-band model may not be a reliable method to detect Lifshitz transitions. We addressed the reported Lifshitz transitions at $T \geq 80$ K in ZrSiSe, which are inferred from the anomalies in the carrier density and mobility in the second band from the two-band model analysis on the Hall magnetoconductivities. We showed that transitions can be artifacts of the fitting, which is overparameterized and can output arbitrary values of the carrier density and mobility for the second band for $T > 80$ K. The unreliability of the two-band model fitting is also affirmed by the large disparities between the experimental longitudinal magnetoconductivity curves and those calculated with the densities and mobilities derived from fitting the longitudinal magnetoconductivity curves [Figs. 2(b) and 2(d)] as well as the entirely different outcomes [Figs. S2(c) and S2(d) in the Supplemental Material [28] vs Figs. 2(e) and 2(f)] when both the longitudinal and Hall magnetoconductivities are fitted simultaneously. It is further attested by the scaling behavior of the MR following the (extended) Kohler's rule, which suggests the absence of anomalies in the carrier densities. In this paper, we demonstrate that caution needs to be taken in interpreting the temperature dependences of the carrier density and mobility derived from the two-band model analysis on magnetoconductivities of a multiband system.

ACKNOWLEDGMENTS

Magnetotransport measurements and data analysis were supported by the U.S. Department of Energy (DOE), Office of Science, Basic Energy Sciences, Materials Sciences and Engineering. Crystal growth at Penn State was supported by the DOE under Grant No. DE-SC0019068. S.E.P. and Z.L.X. received support from the National Science Foundation (Grant No. DMR-1901843). Work performed at the Center for Nanoscale Materials, a DOE Office of Science User Facility, was supported by the DOE, Office of Basic Energy Sciences, under Contract No. DE-AC02-06CH11357.

- [1] I. M. Lifshitz, *Sov. Phys. JETP* **11**, 1130 (1960).
- [2] D. Aoki, G. Seyfarth, A. Pourret, A. Gourgout, A. McCollam, J. A. N. Bruin, Y. Krupko, and I. Sheikin, *Phys. Rev. Lett.* **116**, 037202 (2016).
- [3] Z. J. Xiang, G. J. Ye, C. Shang, B. Lei, N. Z. Wang, K. S. Yang, D. Y. Liu, F. B. Meng, X. G. Luo, L. J. Zou *et al.*, *Phys. Rev. Lett.* **115**, 186403 (2015).

- [4] M. Krottenmuller, M. Vöst, N. Unglert, J. Ebad-Allah, G. Eickerling, D. Volkmer, J. Hu, Y. L. Zhu, Z. Q. Mao, W. Scherer *et al.*, *Phys. Rev. B* **101**, 081108(R) (2020).
- [5] G. Bastien, A. Gourgout, D. Aoki, A. Pourret, I. Sheikin, G. Seyfarth, J. Flouquet, and G. Knebel, *Phys. Rev. Lett.* **117**, 206401 (2016).

- [6] C. Liu, T. Kondo, R. M. Fernandes, A. D. Palczewski, E. D. Mun, N. Ni, A. N. Thaler, A. Bostwick, E. Rotenberg, J. Schmalian *et al.*, *Nat. Phys.* **6**, 419 (2010).
- [7] Y. Liu, Y.-F. Liu, X. Gui, C. Xiang, H.-B. Zhou, C.-H. Hsu, H. Lin, T.-R. Chang, W. Xie, and S. Jia, *Proc. Natl. Acad. Sci. USA* **117**, 15517 (2020).
- [8] Y. Wu, N. H. Jo, M. Ochi, L. Huang, D. Mou, S. L. Bud'ko, P. C. Canfield, N. Trivedi, R. Arita, and A. Kaminski, *Phys. Rev. Lett.* **115**, 166602 (2015).
- [9] Y. Zhang, C. Wang, L. Yu, G. Liu, A. Liang, J. Huang, S. Nie, X. Sun, Y. Zhang, B. Shen *et al.*, *Nat. Commun.* **8**, 15512 (2017).
- [10] F. C. Chen, Y. Fei, S. J. Li, Q. Wang, X. Luo, J. Yan, W. J. Lu, P. Tong, W. H. Song, X. B. Zhu *et al.*, *Phys. Rev. Lett.* **124**, 236601 (2020).
- [11] S. Y. Back, Y.-K. Kim, H. Cho, M.-K. Han, S.-J. Kim, and J. S. Rhyee, *ACS Appl. Energy Mater.* **3**, 3628 (2020).
- [12] L. S. Sharath Chandra, S. K. Ramjan, S. Banik, A. Sagdeo, and M. K. Chattopadhyay, *Appl. Phys. Lett.* **118**, 143905 (2021).
- [13] K. Kang, W. J. Kim, D. Kim, S. Kim, B. Ji, D. H. Keum, S. Cho, Y.-M. Kim, S. Lebègue, and H. Yang, *Adv. Mater.* **33**, 2005742 (2021).
- [14] Y. Tian, Y. Zhu, R. Li, Z. Q. Mao, and J. H. Ross Jr., *Phys. Rev. B* **104**, L041105 (2021).
- [15] H. F. Yang, L. X. Yang, Z. K. Liu, Y. Sun, C. Chen, H. Peng, M. Schmidt, D. Prabhakaran, B. A. Bernevig, C. Felser *et al.*, *Nat. Commun.* **10**, 3478 (2019).
- [16] S. Beaulieu, S. Dong, N. Tancogne-Dejean, M. Dendzik, T. Pincelli, J. Maklar, R. P. Xian, M. A. Sentef, M. Wolf, A. Rubio *et al.*, *Sci. Adv.* **7**, eabd9275 (2021).
- [17] R. J. Kirby, L. Muechler, S. Klemen, C. Weinberg, A. Ferrenti, M. Oudah, D. Fausti, G. D. Scholes, and L. M. Schoop, *Phys. Rev. B* **103**, 205138 (2021).
- [18] M. Yang, Y. D. Liu, W. Zhou, C. Liu, D. Mu, Y. N. Liu, J. Wang, W. C. Hao, J. Li, J. X. Zhong *et al.*, *ACS Nano* **16**, 3036 (2022).
- [19] J. Song, M. Song, Z. Li, J. Wang, Y. Wang, L. Zhang, Y. Han, L. Cao, Y. Xiong, and D. Liu, *Phys. Rev. B* **103**, 165141 (2021).
- [20] X. Wang, D. Pan, Q. Zeng, X. Chen, H. Wang, D. Zhao, Z. Xu, Q. Yang, J. Deng, T. Zhai *et al.*, *Nanoscale* **13**, 2601 (2021).
- [21] X. C. Yang, X. Luo, J. J. Gao, Z. Z. Jiang, W. Wang, T. Y. Wang, J. G. Si, C. Y. Xi, W. H. Song, and Y. P. Sun, *Phys. Rev. B* **104**, 155106 (2021).
- [22] Y. Jian, Q. S. Wu, M. Yang, Q. Feng, J. X. Duan, D. Y. Chen, Q. S. Wang, W. D. Xiao, Y. G. Shi, O. V. Yazyev *et al.*, *2D Mater.* **8**, 015020 (2021).
- [23] E. Cheng, W. Xia, X. Shi, H. Fang, C. Wang, C. Xi, S. Xu, D. C. Peets, L. Wang, H. Su *et al.*, *Nat. Commun.* **12**, 6970 (2021).
- [24] K. Majhi, V. Kakani, R. Ganesan, and P. S. Anil Kumar, *Appl. Phys. Lett.* **120**, 093105 (2022).
- [25] J. Xu, F. Han, T.-T. Wang, L. R. Thoutam, S. E. Pate, M. D. Li, X. F. Zhang, Y.-L. Wang, R. Fotovat, U. Welp *et al.*, *Phys. Rev. X* **11**, 041029 (2021).
- [26] J. Hu, Z. J. Tang, J. Y. Liu, X. Liu, Y. L. Zhu, D. Graf, K. Myhro, S. Tran, C. N. Lau, J. Wei *et al.*, *Phys. Rev. Lett.* **117**, 016602 (2016).
- [27] <https://www.originlab.com/>.
- [28] See Supplemental Material at <http://link.aps.org/supplemental/10.1103/PhysRevB.107.035104> for additional analysis results including two-band and three-band model analysis with fittings of both longitudinal and Hall magnetoelectroconductivities simultaneously as well as (extended) Kohler's rule plots.
- [29] L. R. Thoutam, S. E. Pate, T. Wang, Y.-L. Wang, R. Divan, I. Martin, A. Luican-Mayer, U. Welp, W.-K. Kwok, and Z.-L. Xiao, *Phys. Rev. B* **106**, 155117 (2022).
- [30] https://www.originlab.com/doc/Origin-Help/Interpret-Regression-Result#Adj_R-Square.
- [31] Y.-C. Chiu, K.-W. Chen, R. Schönemann, V. L. Quito, S. Sur, Q. Zhou, D. Graf, E. Kampert, T. Förster, K. Yang *et al.*, *Phys. Rev. B* **100**, 125112 (2019).
- [32] J. P. Song, J. Wang, Y. H. Wang, L. Zhang, M. Song, Z. H. Li, L. Cao, D. Y. Liu, and Y. M. Xiong, *J. Appl. Phys.* **131**, 065106 (2022).
- [33] F. Han, J. Xu, A. S. Botana, Z. L. Xiao, Y. L. Wang, W. G. Yang, D. Y. Chung, M. G. Kanatzidis, M. R. Norman, G. W. Crabtree *et al.*, *Phys. Rev. B* **96**, 125112 (2017).